analytical chemistry

Article

pubs.acs.org/ac

Dynamics of Redox Processes in Ionic Liquids and Their Interplay for Discriminative Electrochemical Sensing

Chunhui Xiao,[†,‡] Abdul Rehman,[†] and Xiangqun Zeng*[,†]

[†]The Department of Chemistry, Oakland University, Rochester, Michigan 48309, United States

[‡]State Key Laboratory of Chemo/Biosensing and Chemometrics, College of Chemistry and Chemical Engineering, Hunan University, Changsha, 410082, China

Ⓢ *Supporting Information*

ABSTRACT: Motivated by the use of ionic liquids (ILs) as green replacers of traditional electrolytes, a mechanistic study has been systematically conducted to comprehend various design principles responsible for electrochemical profiling of redox-active species in ILs. The full spectrum of properties associated with ILs is exploited to assess the viability of this platform, thus revealing the correlation between the redox properties and the physiochemical parameters of the species involved. This includes the evaluation of (1) the variation of redox responses toward analytes with similar molecular structures or functionalities of ILs, (2) the influence in terms of physical criteria of the system such as viscosity and conductivity as well as chemical structure of ILs, and (3) the sustainability in harsh conditions (high temperature or humidity) and interferences. The principle is exemplified via trinitrotoluene (TNT) and dinitrotoluene (DNT) with inherent redox activity as analytes and IL membranes as solvents and electrolytes using glassy carbon (GC) electrodes. A discrete response pattern is generated that is analyzed through linear discriminant analysis (LDA) leading to 100% classification accuracy even for the mixture of analytes. Quantitative analysis through square wave voltammetry (SWV) gave rise to the detection limits in liquid phase of 190 and 230 nM for TNT and DNT, respectively, with a linear range up to 100 μM. Gas-phase analysis shows strong redox signals for the estimated concentrations of 0.27 and 2.05 ppm in the gas phase for TNT and DNT, respectively, highlighting that ILs adopt a role as a preconcentrator to add on sensitivity with enhanced selectivity coming from their physiochemical diversity, thus addressing the major concerns usually referred to most sensor systems.

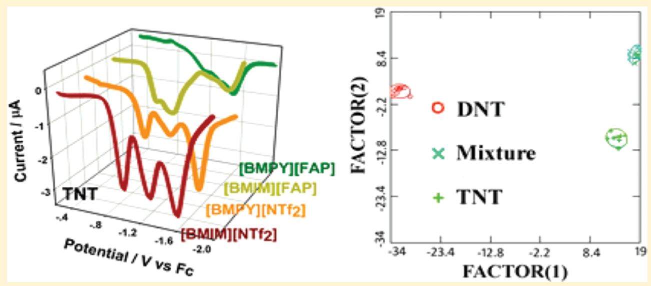

The modern scientific world is largely actuated by the terms "green" and "miniaturized" when it comes to the sensor systems. Electrochemical techniques are equipped with inherent advantages to be incorporated into small portable devices, but a number of problems associated with conventional solvents and electrolytes used in electrochemical methods render them unsuitable for facile and green technologies.[1] Common electrolytes are classified as liquid electrolytes (aqueous electrolyte, nonaqueous electrolyte) and solid electrolytes.[2,3] Liquid electrolytes possess highly charged carriers but have the problem of volatility of the solvents that can lead to the exhaustion of the solvents during the reaction. The solid electrolytes overcome the problem of leakage of the solvents, but they cannot supply high electrical conductivity at room temperature due to either an insufficient number of electrical carriers or low ionic mobility.[4] Due to their inherent ionic conductivity and wide electrochemical window (up to 5.5 V),[5] ionic liquids (ILs) are adapting the role of green solvents and electrolytes in electrochemical measurements.[6−9] With innate electrolytic and specific solvation traits, ILs provide an efficient solution to be employed in various analytical applications,[10] particularly in gas sensing.[11,12] In addition, their excellent thermal stability (even up to 350 °C), negligible volatility, and noninflammability enable regeneration and purification prior to the experiments easier via thermal treatment of the IL electrolytes, which is very important for field applications. More importantly, the synthetic flexibility allows ILs to be tailored with a broad chemical diversity, which facilitates us to design selective IL electrochemical sensor arrays and to explore their applications for the detection and classification of redox-active compounds with the help of pattern recognition algorithms.

Indeed, ILs possess a number of unique physiochemical attributes that could provide electrochemical selectivity including tunable viscosity and varying solvation properties in comparison to traditional organic electrolytes,[13] which determines the diffusion and mass transport behavior of electroactive organic species in ILs. Viscosity is one of the key factors in this regard. As per Walden's rule, there is an inverse relationship between conductivity and viscosity

Received: September 21, 2011
Accepted: December 16, 2011
Published: December 16, 2011

regardless of temperature.[14] ILs with a large range of viscosities and conductivities can definitely affect the mass transport and electron-transfer rates and may provide entirely different electrochemical responses. Second, unique solvent properties of ILs can support many different types of solvent−solute interactions, such as hydrogen bonding, $\pi-\pi$ interactions, and ion pair solvation, which are multiplexed through the presence of different analyte structures, significantly affecting the redox processes, thus generating a highly selective response pattern. Solvation properties of ILs enable them to be ideally suited as a sensing platform which is depicted from our previous work as well as the vapor-phase experiments herein.[15] In addition, ILs can also act as preconcentrators for the analytes. This feature can be explored to enhance the sensitivity but also the selectivity determined by ILs−analyte interactions as demonstrated in this work. All these factors pose an obsessive demand for strong background information which is being reported in this work, to show how different analytes undergo redox reactions in these complex media and generate sensing signals. Electrochemical investigations are carried out systematically to study the role of different IL structures in electron-transfer processes which facilitate us to design an array of IL sensors which can be generalized for various targets suitable for electrochemical detection. The range of selected ILs includes a variety of ILs that vary in terms of physical properties, protonation capabilities, and interaction possibilities to offer so that the parameters involved can be identified for electrochemical detection. Four different ILs, based on both imidazolium and pyrrolidinium anions, are utilized, and their properties are shown in Table 1 from the published data.[16−18]

Table 1. Chemical and Physical Properties of ILs (20 °C)

ILs	viscosity (cP)	molar mass (g/mol)	density (g/cm^3)	conductivity (mS/cm)
[BMIM[NTf$_2$]	54	419.37	1.44	3.7
[BMPY][NTf$_2$]	79	422.41	1.40	2.4
[BMIM][FAP]	93	584.23	1.63	2.3
[BMPY][FAP]	292	587.27	1.59	0.9

Redox activity associated with nitro explosives and their widespread exploitation by the terrorists beyond the political boundaries in recent years[19] strongly argue for their selection as the model analytes for the present study, an intriguing choice for a variety of concerns. Surface modifications of electrodes by employing metal nanoparticles,[20] carbon nanotubes,[21] functionalized mesoporous silica,[22] and graphene[23] have been put forward as a solution in recent years, but the practical use is limited by multiple procedural manipulations. For these reasons, nitro explosives are the best starting point[24,25] which can assist to counter these threats and to provide a continued surveillance with already existing targets of humanitarian demining, remediation of waste sites, and forensic demands. Explosive representatives used in this work include trinitrotoluene (TNT), the most widely used military explosive and highly difficult target for sensing protocols owing to its low vapor pressure, dinitrotoluene (DNT), frequently found at ammunitions-contaminated sites, and a mixture of TNT and DNT (molar ratio = 1:1), since these two compounds are commonly found together in real-world samples.[26] The performance of different IL sensors in an electrochemical sensor array with respect to sensitivity, linear range, and selectivity toward nitroaromatic compounds is evaluated and discussed in order to demonstrate the applicability of the IL sensor array platform for the classification of TNT, DNT, and their mixture.

■ EXPERIMENTAL DETAILS

Chemicals. 1-Butyl-3-methylimidazolium bis(trifluoromethanesulfonyl)imide [BMIM][NTf$_2$] and 1-butyl-1-methylpyrrolidinium bis(trifluoromethanesulfonyl)imide [BMPY][NTf$_2$] were synthesized by Dr. Gary Baker at the University of Missouri,[27] with 98% purity, whereas 1-butyl-3-methylimidazolium tris(pentafluoroethyl)trifluorophosphate [BMIM][FAP] was obtained from Merck KGaA. 1-Butyl-1-methylpyrrolidinium tris(pentafluoroethyl)trifluorophosphate [BMPY][FAP] was synthesized by Dr. Jared Anderson at the University of Toledo.[18] The explosive compounds TNT (99.5%, Chem Service), DNT (97%, Sigma-Aldrich), and nitromethane (NM) (98.5%, Sigma-Aldrich) were used as received without further purification. Nitroglycerin (NG) was prepared in our lab by the reported procedure.[28] This procedure is carried out with extreme care, and a small quantity (~500 μL) of the explosive is synthesized at one time and cautiously stored in refrigerator until further use. Chemical structures of the ILs and the analytes are given in Supporting Information Figure S1.

Preparation of the IL Sensor Array. Prior to use, glassy carbon (GC) electrodes (diameter = 3 mm) were carefully polished to a mirror-like plane with 0.5 and 0.05 μm alumina slurries, successively. Afterward, the GC electrodes were washed thoroughly with excess amounts of water and ethanol, respectively, and then dried under nitrogen gas.

Without specific description, analytes were initially in the liquid phase. An amount of 200 μL of the respective IL was drop-coated onto the working electrode inside a Kel-F electrochemical cell which is purposefully designed to facilitate the proper positioning of a three-electrode system. Solutions with specified concentrations of nitro compounds were prepared by directly dissolving them in the same ionic liquid and were introduced as a thin electrolytic membrane.

For vapor-phase sensing, 15 μL of the selected ILs was coated onto the surface of the GC electrode to form a thin liquid layer. The explosive vapors were generated by flowing specific amounts of N_2 gas through the solid powdered analytes, and an approximation of the concentrations can be achieved via the ideal gas laws as well as the reported vapor pressures for those analytes. The measurement cell was joined to a 50 cm^3 gas container, and about 10 mg of the sample powder was spread at its bottom to achieve complete saturation. The system was heated to 50 °C to reach the detectable concentration, whereas the IL layer thickness was very thin for facile adsorption and mass transport.

For the evaluation of humidity influences, a mass flow controller setup is designed where the concentration of water was adjusted by controlling the amount of N_2 flowing through distilled water and mixing it with dry N_2. The temperature of the system was controlled through water baths which kept the water circulating around the cell with attached accessories.

Electrochemical Measurements. All electrochemical measurements were performed on a CHI 1000A electrochemical workstation (CH Instrument, Inc. U.S.A.) with a three-electrode system comprising a platinum wire as an auxiliary electrode, a fresh silver wire as the quasi-reference electrode, and a GC electrode as the working electrode. The distance from the tip of the Ag quasi-reference electrode to the

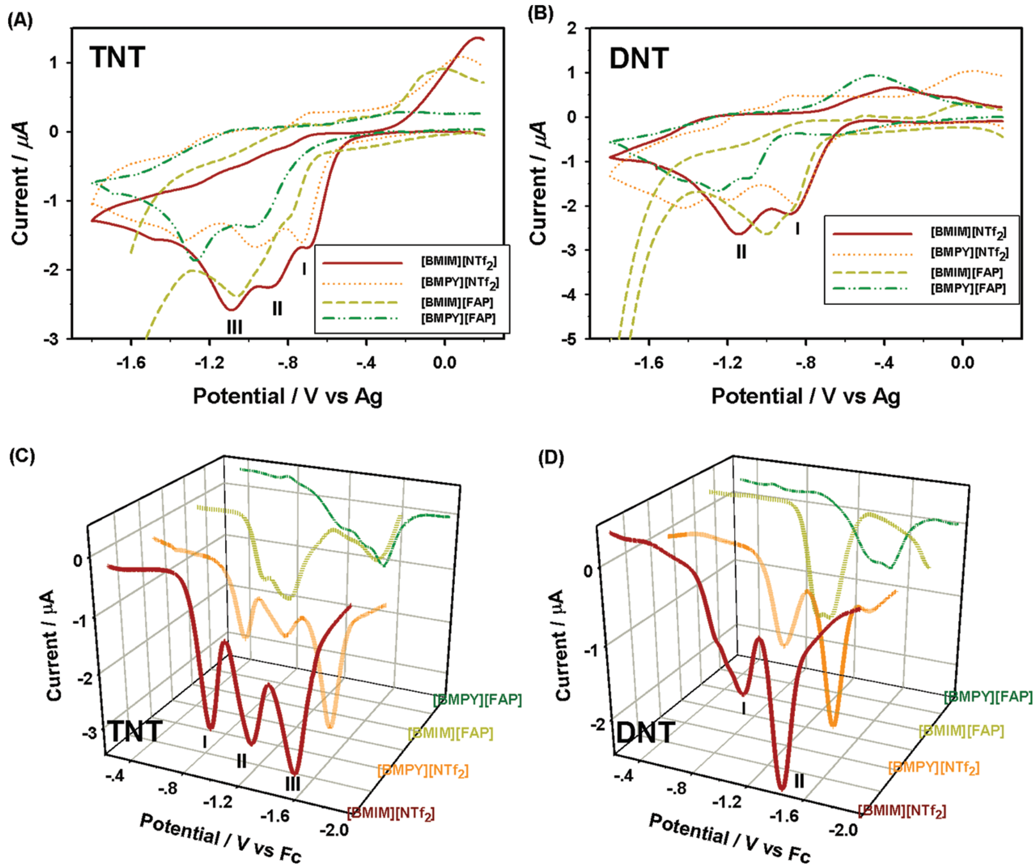

Figure 1. Background-subtracted cyclic voltammograms for 0.1 mM TNT (A) and 0.1 mM DNT (B) in different ILs. Scanning rate: 100 mV/s. Background-subtracted square wave voltammograms for TNT (C) and DNT (D) in different ILs.

center of the GC working electrode was set at 2 mm to minimize the effects of uncompensated electrolyte resistance. Although the potential scales could be established for some ionic liquids using Fc/Fc^+ couples, adsorption and chemical reactions coupled to the charge-transfer process may cause uncertainty in this calibration. Therefore, we only used 50 μM Fc/Fc^+ calibrated potential for square wave voltammetry (SWV) for 0.1 mM TNT and DNT in four different ILs, which is shown in Figure 1, parts C and D, but kept the other potential scales versus a Ag quasi-reference electrode. A schematic diagram of the electrochemical cell is illustrated in Scheme 1. Electrochemical experiments were performed in ILs deoxygenated by bubbling highly pure nitrogen for more than 30 min while this N_2 flow was maintained during measurements as well. Square wave voltammetry was done with an amplitude of 25 mV and frequency of 30 Hz. The reduction signals of the different concentrations of analytes were corrected by subtracting the background current directly. Individual peak current was used in most of the cases to analyze the voltammetry data, but total peak area was used for analysis of the voltammetry data for analytes such as NG and NM with low redox sensitivity and in ILs with broadened redox peaks. As shown in Supporting Information Figure S2, this simple method of correction does not change the real value of reduction response, but it could be helpful for us to obtain more accurate values about reduction peak areas and currents.

Scheme 1. Side View Schematic Diagram of the Electrochemical Cell for Both Liquid and Gas Phases (Not to Scale)[a]

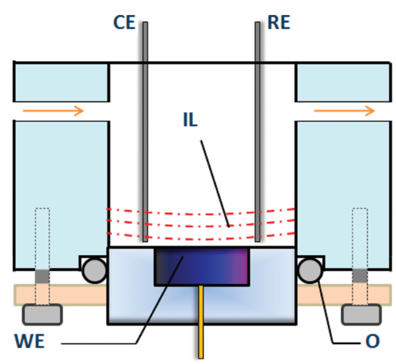

[a]Abbreviations: CE, counter electrode; IL, ionic liquid; O, O-ring; RE, reference electrode; WE, working electrode.

RESULTS AND DISCUSSION

Electrochemical Redox Processes of TNT and DNT in ILs. Cyclic voltammetry (CV) and SWV studies in four different ILs were carried out in order to characterize the electrochemical behavior of the analytes. CV is a powerful tool in the studying of electrode reaction mechanisms, whereas SWV is utilized for the quantifications of trace analytes due to the lesser contribution of capacitative charging current in SWV. Parts A and B of Figure 1 show the CV curves of 0.1 mM TNT and DNT in the selected ILs on the GC electrode at a scan rate of 100 mV/s, which demonstrate the redox activities of both of these explosives in the IL media, already forming a selectivity pattern based upon the nature of the IL used.

Scheme 2. Proposed Mechanism of Reduction of Nitroaromatic Compounds via Six Electron-Transfer Processes

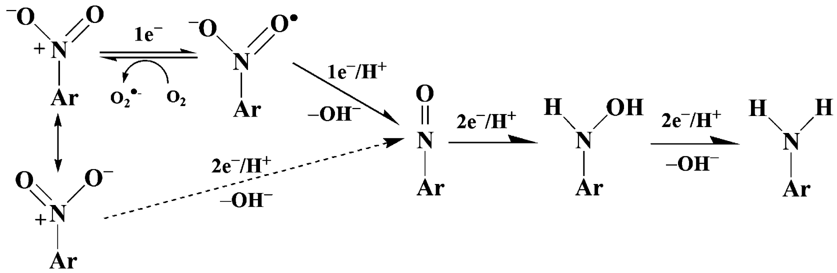

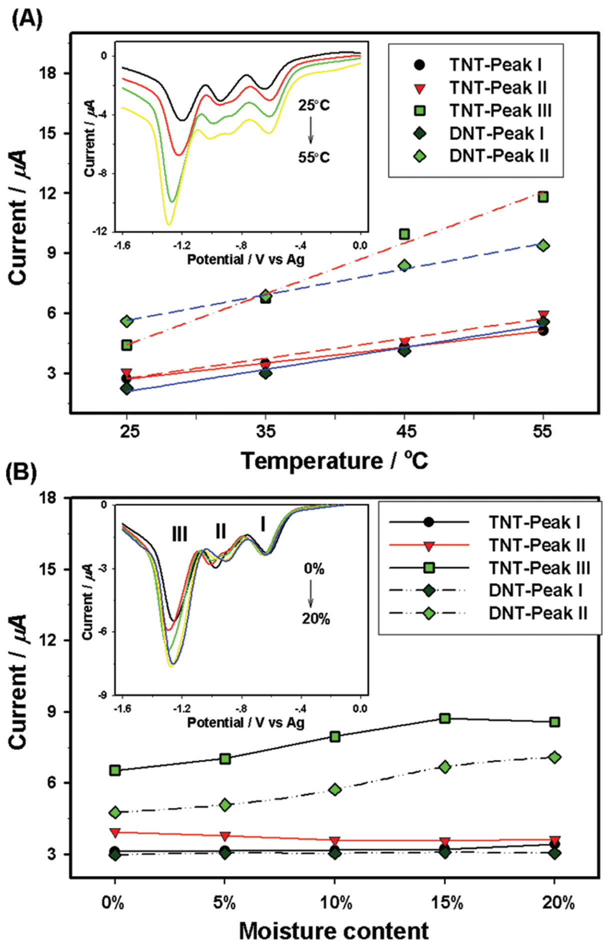

Figure 2. (A) Current changes of cathodic peaks I, II, and III for 0.2 mM TNT and peaks I and II for 0.2 mM DNT in $[BMPY][NTf_2]$ at different temperatures. Inset: representative SWV curves for TNT at different temperatures. (B) Current changes of cathodic peaks I, II, and III for 0.2 mM TNT and peaks I and II for 0.2 mM DNT in $[BMPY][NTf_2]$ under different moisture levels. Inset: representative SWV curves for TNT under different moisture levels.

This pattern is similar to what is observed when the measurements are carried out in aqueous solution, demonstrating that the general nature of electrochemical processes of these analytes is not modified considerably. According to the currently accepted mechanism, as shown in Scheme 2,[22,29−32] at first, a radical anion is yielded from a one-electron reduction, and then three irreversible reduction processes involving the addition of five electrons and three protons at more negative potentials occur, which proceed via the generation to nitroso, hydroxylamine, and amine.

Parts C and D of Figure 1 compare the SWV curves toward 0.1 mM TNT and DNT in four selected ILs, which illustrates the formation of visual patterns showing that not only the amperometric responses but also the nature of reduction peaks toward nitroaromatics is significantly different in the four different ILs. These measurements have led us to conclude the emergence of the following trends: (1) on the basis of the same anions, reduction peak currents in $[BMIM]^+$-based ILs are apparently higher than those in $[BMPY]^+$; (2) curves in two $[NTf_2]^-$-based ILs show well-defined reduction peaks corresponding to the number of nitro functions in TNT and DNT, whereas in [BMIM][FAP] and [BMPY][FAP], they display broadened peaks, most probably a consequence of peak overlapping.

The above observations can be explained on the basis of possible protonation effects produced either by IL cations or by the traces of residual water. (The water molecules in IL are structurally associated with the ions of the ILs and therefore difficult to remove completely. Typically, the removal of water from the IL and the readsorption of water from air have reached equilibrium when N_2 purging is carried out on benchtop conditions.) After the first reduction of the nitro group, at more negative potential, one more electron is added into the analyte molecule generating a highly unstable dianion. Owing to the great reactivity of this dianion, it undergoes rapid protonation with loss of a water molecule[33] and is converted into nitrosoaryl molecules. It is believed that this dianion is a strong Lewis base capable of removing protons from species which are not proton donors under normal conditions. There are enough proton sites on $[BMIM]^+$, i.e., a readily available acidic proton at the C(2) position and two protons at the ring which have also been shown to be exchangeable.[34] In comparison, for $[BMPY]^+$, the protons are harder to remove, which may contribute to the lower reduction peak currents shown in ILs with $[BMPY]^+$ cations.

Another significant factor that contributes to the above observations is the varying viscosity of the ILs which is inversely related to the conductivity. By position of the Ag reference electrode close to GC working electrode, the uncompensated resistance or ohmic (IRu) drop in ILs can be minimized. However, the viscosity of ILs plays a significant role in the mass transport of the radicals formed. Once a functional group is reduced to amino functionality, further reduction of the nitro groups still present on the molecule becomes increasingly difficult, as explained in the previous discussion that adds upon the hindered mass transport. These two factors combine together to produce the peak overlapping in case of [FAP]-based ILs. Due to peak overlapping in some of ILs used, we calculated peak areas for all reduction peaks based on the experimental results. They are in the following order: $[BMIM][NTf_2]$ > $[BMPY][NTf_2]$ > [BMIM][FAP] >

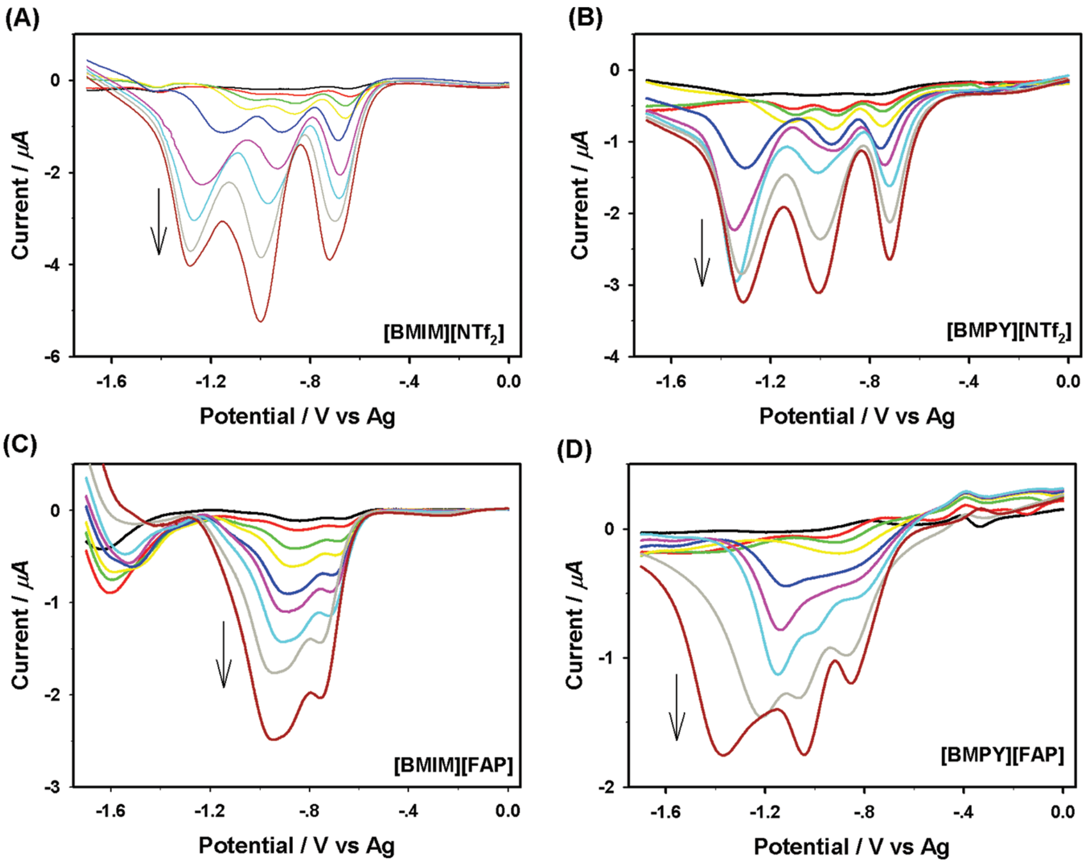

Figure 3. Square wave voltammograms in ILs containing different concentrations of TNT (from top to bottom): 5, 10, 20, 30, 50, 70, 100, 150, 230 μM, respectively.

[BMPY][FAP] as plotted in Supporting Information Figure S3. The listed physical and chemical properties of as-used ILs in Table 1 display a strong correlation to the response patterns. The order of viscosity and conductivity of ILs is entirely matched with peak areas, thus defining their role in the electrolytic reduction of nitroaromatics. Lower viscosity leads to higher conductivity and fast mass transport, which is a vital component in designing successful electrochemical sensors.

In addition to viscosity, there are several other factors that can influence the mechanistic profiles observed. One of the responsible factors is the solvation effect. The relative permittivity of ILs falls in a very high range, which has a decisive influence on the interactions between the IL and the analyte species involved in the process. Although the conventional solvent systems do possess these variations in relative permittivity and solvation dynamics, it is magnified in case of ILs because of large differences in their tunable structure−property relationships. So the diffusion coefficients of various charged intermediates vary significantly. That is why the ratio between peak currents is also changed with the change of electrolyte structure. For example, the ratios between the first and the last peaks are quite different in [BMIM][NTf_2], i.e., TNT (0.9) to DNT (0.5), whereas in [BMPY][NTf_2], these are almost the same (around 0.5). These variations are quite beneficial to design a discriminatory system for analyte combinations.

IL as a solvent plays an active role in dispersing the solute into individual molecules through many types of solvation force, which is predominantly hydrogen bonding in this case. We hypothesize that there is a competition between the anion and nitroaromatics (NACs) including initial reactant and its reduction products for the proton, as shown in eqs 1 and 2.

$$C^+ + A^- \overset{K_1}{\Leftrightarrow} C^+ \cdots A^-, \qquad K_1 = \frac{[C^+ \cdots A^-]}{[C^+][A^-]} \tag{1}$$

$$C^+ + \text{NACs} \overset{K_2}{\Leftrightarrow} C^+ \cdots \text{NAC}, \qquad K_2 = \frac{[C^+ \cdots \text{NACs}]}{[C^+][\text{NACs}]} \tag{2}$$

Clearly the concentration of hydrogen-bonded $C^+ \cdots$NACs complex is dependent upon the availability of cation as hydrogen-bonding donor and anions including NACs as hydrogen-bonding acceptor. Since hydrogen-bond donation increases with the increasing s-character of the C−H bond,[35,36] the K_1 values in imidazolium ILs are usually lower than those in pyrrolidinium ILs with similar substitution, thus increasing the concentration of free nonbonding C^+ and $C^+ \cdots$NACs complex, which leads to enhanced electrolytic performance. As for anions of ILs, although the presence of $[FAP]^-$ leads to an enhancement of the hydrogen-bond acidity relative to the $[NTf_2]^-$ analogues,[37,38] higher viscosity and low conductivity still depress electrochemical response in $[FAP]^-$-based ILs. TNT possesses better proton-accepting ability than DNT since a trinitroaromatic compound has one more substitution allowing it to be reduced easier than dinitro compounds. This is visible as all of the reduction peaks of DNT appear more negative in comparison with that of TNT.

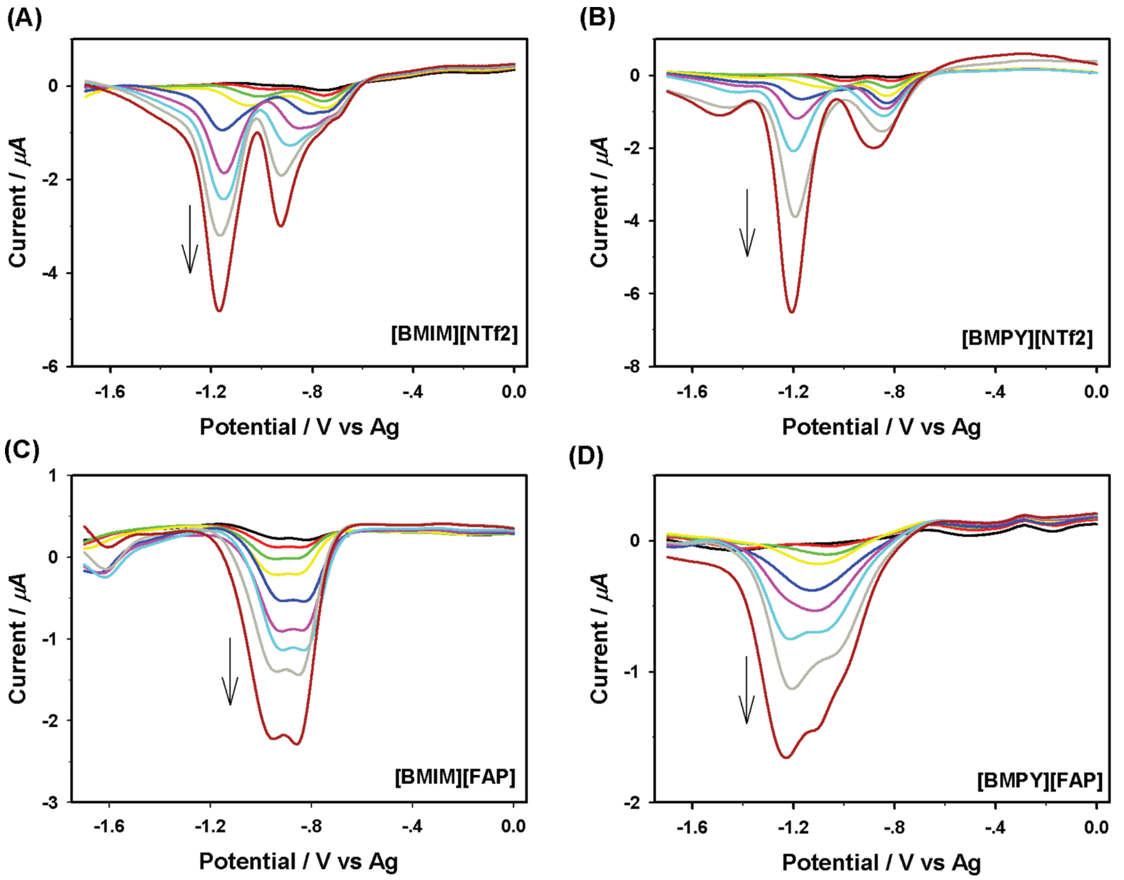

Figure 4. Square wave voltammograms in ILs containing different concentrations of DNT (from top to bottom): 5, 10, 20, 30, 50, 70, 100, 150, 230 μM, respectively.

CV was also performed at different scan rates, and the results are combined in Supporting Information Figures S4 and S5, which show that the reduction peaks of TNT and DNT are proportional to the square root of the scan rate, which means that the reduction process for this type of system is diffusion-controlled. Therefore, the mass transport, which was governed by the viscosity of ILs as well as the interaction forces between the involved components of the system, would play a key role in the electrochemical reduction of the two selected nitro-aromatics.

Enhanced Analytical Performance under Atmospheric Variations. For a sensing protocol to be used for any practical purpose, its workability in real-life conditions must be elucidated. The high thermal stability of ILs makes them excellent materials for high-temperature applications. The effect of temperature on the electrochemical sensor is investigated using 200 μM TNT or DNT as standard conditions. In both cases, all the reduction peak currents increased systematically with temperature, as shown in Figure 2A. Several factors can contribute to the temperature-dependent current response in ILs. The first one is viscosity. The IL viscosity decreases as its temperature increases.[39] A recent work shows that viscosity can be described by a simple linear equation: $(1/\eta)^{\phi} = a + bT$ in which a and b are constants and ϕ is a characteristic exponent.[40] It was shown that this equation fits many ILs including the NTf_2 ones used in our study with $\phi = 0.300$. The second is the temperature-dependent diffusion coefficient, which also depends on dynamic viscosity of the solvent described empirically by the Stokes–Einstein equation. The third is the temperature- dependent mass transfer to an electrode. It was reported that heating of the electrode can induce convection in solution and thermal gradients at the electrode–electrolyte interface.[41,42] The increased thermal energy of the interacting molecules due to increase of temperature can also facilitate the solvation process that can contribute to the increase of current observed. We observed a linear relationship between the response of the first peak and temperature for TNT and DNT which are $Ip_{,TNT}$ (μA) = 0.70 + 0.08T (°C) (R^2 = 0.9995) and $Ip_{,DNT}$ (μA) = −0.68 + 0.11T (°C) (R^2 = 0.9812), respectively. The experimentally observed linearity is likely the nonlinear combination of all these factors. Nevertheless, the temperature effect on redox current leads to increased sensitivity of voltammetric method, which may prove to be a great advantage for trace analysis.

The efficiencies of the as-mentioned ILs to respond to nitro compounds under the scenario of large variations in relative humidity were also investigated as shown in Figure 2B. With increase in moisture content of the system from 0% to 20%, we observed changes of peak current only for the last peak, which is commonly related to the availability of protons in the electrolyte solutions. Therefore, the existence of water, a proton donor, is definitely going to affect the final reduction of nitro compounds in addition to the cations of ILs, which can also serve as proton source, as discussed earlier. The representative background-subtracted SWV curves for 200 μM TNT with different amounts of water in the inset of Figure 2B describes the fact that the first peak current and potential is independent of water contamination in the electrolyte. Hence, the first

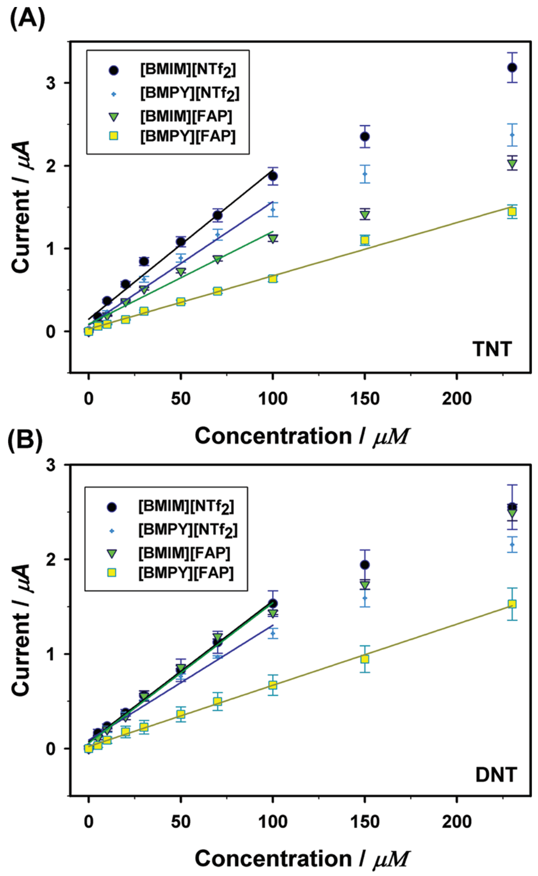

Figure 5. Plot of current changes from cathodic peak I vs concentrations for TNT (A) and DNT (B).

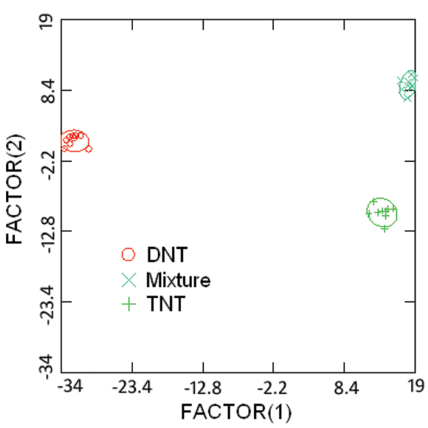

Figure 6. LDA canonical scores plot of the three analytes with different concentrations tested against the ILs sensor array by nine replicate data sets.

reduction peak was used for our sensing calibration, since it is more reversible and stable and is not affected by the concentration of proton, as demonstrated in these samples.

Effect of Interferences. We have evaluated the viability of the proposed methods against other nitro explosives (NM and NG) under the standard conditions. NM and NG can behave as interferences in real-world conditions. For the same concentration of analytes (100 μM), it is found that the values of reduction peak area toward these compounds have the following order: TNT > DNT ≫ NM > NG, and the ratio is 106:80:1.5:1. The value of peak area was used here for comparison, since it gives enhanced sensitivity and reflects the whole redox property based on Faraday's law ($Q = nFN$). Much higher sensitivity for TNT and DNT is mainly ascribed to the presence of aromatic rings which make nitro functions to be better proton acceptors, and hence, higher response observed. Additionally, the selected ILs, all contain aromatic ring structures which provide better solubility for the aromatic compounds and prove a mean for faster mass transport. This result not only proves the enhanced selectivity using ILs in comparison to routine electrolytes but also prompts us to tailor the functionalized ILs structures for specific analyte and circumstantial demands.

Profiling of Sensory Performance. *Quantitative Evaluation and Pattern Analysis.* Figures 3 and 4 show representative sensograms for different concentrations of TNT and DNT, respectively (230−5 μM), in four ILs. Obviously, in all cases, the peak intensity decreases with the decrease of concentration of the analytes while the peak potentials shift toward more positive values. However, when the concentrations are at the lowest level, the reduction peaks are still visible and can be identified. The data for the first reduction peak for various concentrations is collected and summarized in Figure 5 as calibration plots. The linearity of response is observed within the concentration range from 5 to 100 μM. The magnitudal order of responses on the first reduction peak for the TNT is [BMIM][NTf_2] > [BMPY]-[NTf_2] > [BMIM][FAP] > [BMPY][FAP], and for the DNT it is [BMIM][NTf_2] ≈ [BMIM][FAP] > [BMPY][NTf_2] > [BMPY][FAP]. To be noted is that the separation between the peaks for DNT reduction in [BMIM][FAP] (~122 mV) is much smaller than in [BMIM][NTf_2] (~268 mV) so that the first peak in [BMIM][FAP] may be the combination of two or three steps, while that in [BMIM][NTf_2] corresponds to one single reduction step. The sensitivities for the TNT and DNT in [BMIM][NTf_2] have the highest values among the chosen ILs, which are found to be 18 and 15 nA/μM, respectively. The corresponding linear function is $Ip_{,\mathrm{TNT}}$ (μA) = 0.1486 + $0.018C_{\mathrm{TNT}}$ (μM) with a correlation coefficient of $R^2 = 0.9892$ and $Ip_{,\mathrm{DNT}}$ (μA) = 0.0731 + $0.0149C_{\mathrm{DNT}}$ (μM) with a correlation coefficient of $R^2 = 0.9977$. Even down to 500 nM, the reduction peak of TNT and DNT in [BMIM][NTf_2] could be observed, and calculated detection limits (S/N = 3) for TNT and DNT are 190 and 230 nM, respectively.

Again for practical application context, one of the key design factors is whether the strategy is feasible for the monitoring of mixtures, which is quite usually the case with nitro explosives. TNT and DNT simultaneously occur in groundwaters, land mines, and workplaces to become a security risk as well as a health hazard in all instances. That is why we tested a mixture of TNT and DNT (molar ratio, 1:1) as another analyte model, and the sensograms obtained are shown in Supporting Information Figure S6. Although the sensograms in ILs toward TNT and DNT above are proven to be an effective method to selectively detect TNT and DNT, the results of which can even be analyzed by visual tracking using number of peaks, SWV responses toward mixture seem to have no additional peaks in comparison with TNT, as reduction peaks coming from DNT are mostly overlapped with peaks of TNT. On the other hand, as shown in these SWV curves, separation of the reduction peaks especially at low concentrations is very small and even overlapped, which may cause difficulties for the classification of these two similar compounds. Therefore, a pattern recognition

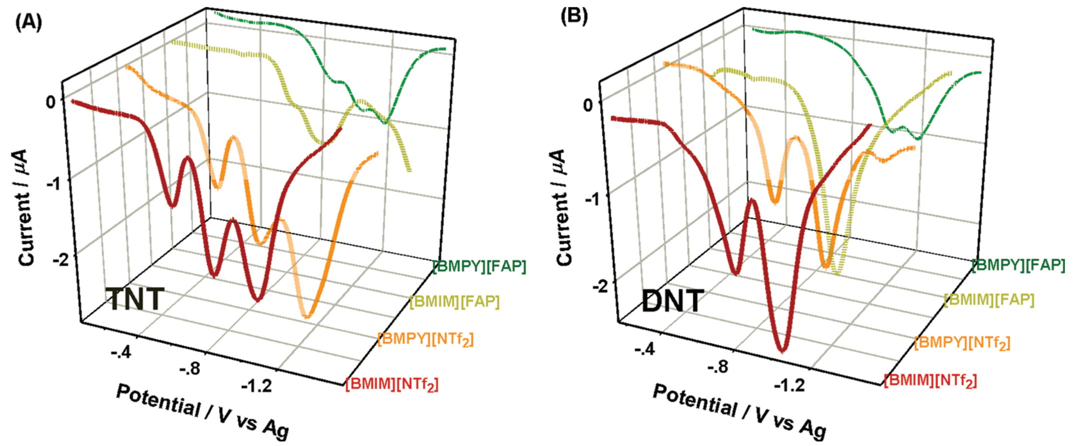

Figure 7. Background-subtracted square wave voltammograms for the vapor of TNT (A) and DNT (B) in different ILs.

algorithm is essentially required for the correct discrimination of representative analytes.

We employed linear discriminant analysis (LDA) as the statistical analytical model in order to get a more easily manageable and visually acceptable two-dimensional chart that contains the distinguishing signals of the original data. LDA is a widely used multivariate analysis technique for transforming the original variables into new, uncorrelated factors. Each factor is a linear combination of the original variables. This methodology helps in dimensionality reduction, classification of samples, and identification of outliers in high-dimensional data.

LDA is routinely applied for the analysis of data where single-point selection is made for each set of measurement profiles, and the test matrix is built on these points, but in comparison, an electrochemical signal is always a two-dimensional chart of varying potential and current and the single-point selection is impossible. This difficulty in modeling the test data set with whole discriminatory information is resolved by setting fixed potential values, and the current is recorded at those values for all measurements. Nine replicate data sets from SWV sensor curves over the concentration range of 5−230 μM for each analyte in each of the ILs are extracted, whereas the representative potentials are 0.5, 0.7, 0.9, and 1.1 V versus Ag. LDA was then applied to uncover characteristic profiles of model analytes by sampling the key feature subsets, scoring each subset for suitable factors, and plotting each sample to a position corresponding to the factor score. As shown in Figure 6, there is no overlap of the data clusters in the canonical factor plots of the LDA results, which indicates excellent sample classification. The sample sets involving the analyte mixture have captured a separate position on the plot rather than mixing with one or both of the analytes, which is tremendously significant. According to our knowledge, scientific literature lacks the examples where the mixtures of the explosive analytes have been so accurately classified, regardless of the fact that both these targets are found together and a correct estimation is essential. The clusters of TNT and mixture of TNT and DNT are closer together, which implies that TNT has the higher impact within the mixture. When it is combined with the higher sensitivity of TNT, a noteworthy fact pops out that the system built with these specific ILs is more feasible to analyze TNT than DNT, which is normally opposite due to the low vapor pressure of TNT. The "jackknifed" classification matrix obtained from this analysis showed 100% accuracy, which is remarkable. When we split the data set into four where each section represents data from each IL, the classification accuracy is yielded to be 85%, 85%, 81%, and 81% for [BMIM][NTf_2], [BMP[NTf_2], [BMIM][FAP], and [BMPY][FAP], respectively, which describes the inherent selectivity hidden inside the IL media as discussed earlier. Nevertheless, considering the diverse structures and properties of ILs, once the selection of the particular set of ILs is optimized, excellent classification or quantification for other potential electrochemically active compounds may also be obtained by this type of IL sensor array.

Explosive Sensing in the Vapor Phase. Another fundamental prerequisite for a promising commercial instrument is the real-world detection capability for gaseous samples. Figure 7 shows the SWVs toward TNT and DNT vapors in four selected ILs, and enhanced responses were obtained comparing with those in liquid phase. Although the approximate concentration at the saturation point via the reported vapor pressures is estimated to be 0.26 ppm (1.2 nM) for TNT and 2.05 ppm (11.3 nM) for DNT, the corresponding solution-phase analyte concentration using the calibration curves obtained in the liquid phase (Figure 5) in [BMIM][NTf_2] for TNT and DNT are 53 and 103 μM, respectively. The collected responses show huge peak currents for such low levels of analyte, which heavily reduced the detection limits. Here, two major factors seem to affect sensitivity amplification, namely, the reduced mass transport distance via the thinner electrolyte layer and the preconcentration of analyte by ILs. The gaseous molecules adsorb quickly into the thinner IL membrane due to faster molecular motions. Furthermore, a greater number of molecules is available at the membrane/electrode interface owing to reduced sample space, thus assisting the sensitivity to be improved. Our previous studies and literature elsewhere demonstrate[15,43] that ILs readily adsorb gas analytes and hence can act as a preconcentrator for these molecules too, expediting the level of analyte at the interfacial boundary. Thus, the proposed strategy herein put forward an effective and sophisticated tool to analyze various nitro explosives both in solution and vapors with great accuracy, whereas the novelty lies in simplified operation and widespread applicability.

■ CONCLUSIONS

Through a systematic study of electrochemical sensing of redox-active explosives in various ILs, we present here a novel method of utilizing the characteristics of ILs for discriminative electrochemical sensing of redox-active compounds. By tuning of cations and anions of ILs to vary the physiochemical properties such as viscosity and conductivity as well as solvation forces like hydrogen-bonding donation ability of ILs, the redox processes of analytes in ILs can be easily tailored to increase the sensitivity and selectivity of electrochemical sensing and discrimination. Using ILs as tunable solvents and electrolytes not only enhances robustness of the analytical sensors but also provides motivation for new specialized designs for these solvents for better sensory devices. The routine sensing protocols were employed including the tests for sensing signals, detection limits, interferences, and environmental interferences. Data analysis is performed for pattern recognition, which showed 100% discrimination accuracy for the model analytes and their mixture. This study intends to pave the way for a systematic approach by the design, selection, and development of ILs for specific analytical applications.

■ ASSOCIATED CONTENT

Ⓢ Supporting Information

Some of the experimental details. This material is available free of charge via the Internet at http://pubs.acs.org.

■ AUTHOR INFORMATION

Corresponding Author

*E-mail: zeng@oakland.edu.

■ ACKNOWLEDGMENTS

We acknowledge an ONR Grant (N000141010734) for supporting this project. We are thankful to Dr. Gary Baker and Dr. Jared Anderson for providing us with ionic liquids used in this study. We also are thankful for Dr. Michael Sevilla's helpful discussion and Dr. Jinhua Chen's encouragement for Chunhui Xiao's visit at Oakland University.

■ REFERENCES

(1) Lund, H. *J. Electrochem. Soc.* **2002**, *149*, S21−S33.
(2) Bhoga, S. S.; Singh, K. *Ionics* **2007**, *13*, 417−427.
(3) Jasinski, P. *Mater. Sci-Poland* **2006**, *24*, 269−278.
(4) Kemula, W.; Krygowski, T. M. In *Encylclopedia of Electrochemistry of the Elements*; Bard, A. J., Lund, H., Eds.; Marcel Dekker: New York, 1979.
(5) Buzzeo, M. C.; Hardacre, C.; Compton, R. G. *ChemPhysChem* **2006**, *7*, 176−180.
(6) Rogers, R. D., Seddon, K. R., Eds.; *Ionic Liquids: Industrial Applications for Green Chemistry*; ACS Sypmposium Series 818; American Chemical Society: Washionton, DC, 2002.
(7) Lagrost, C.; Preda, L.; Volanschi, E.; Hapiot, P. *J. Electroanal. Chem.* **2005**, *585*, 1−7.
(8) Silvester, D. S.; Wain, A. J.; Aldous, L.; Hardacre, C.; Compton, R. G. *J. Electroanal. Chem.* **2006**, *596*, 131−140.
(9) Wang, Z.; Lin, P.; Baker, G. A.; Stetter, J.; Zeng, X. *Anal. Chem.* **2011**, *83*, 7066−7073.
(10) Kroon, M. C.; Buijs, W.; Peters, C. J.; Witkamp, G.-J. *Green Chem.* **2006**, *8*, 241−245.
(11) Díaz Aguilar, A.; Forzani, E. S.; Leright, M.; Tsow, F.; Cagan, A.; Iglesias, R. A.; Nagahara, L. A.; Amlani, I.; Tsui, R.; Tao, N. J. *Nano Lett.* **2009**, *10*, 380−384.
(12) Yu, L.; Huang, Y.; Jin, X.; Mason, A. J.; Zeng, X. *Sens. Actuators, B* **2009**, *140*, 363−370.
(13) Lagrost, C.; Hapiot, P.; Vaultier, M. *Green Chem.* **2005**, *7*, 468−474.
(14) Liu, H.; Liu, Y.; Li, J. *Phys. Chem. Chem. Phys.* **2010**, *12*, 1685−1697.
(15) Rehman, A.; Hamilton, A.; Chung, A.; Baker, G. A.; Wang, Z.; Zeng, X. *Anal. Chem.* **2011**, *83*, 7823−7833.
(16) *Ionic Liquids Today*, 2011, 1−11. http://www.iolitec.com
(17) Merck Product Brochure. http://www.merck-chemicals.com/showBrochure/200910.245.ProNet.pdf.
(18) Yao, C.; Pitner, W. R.; Anderson, J. L. *Anal. Chem.* **2009**, *81*, 5054−5063.
(19) Terrorist attacks throughout the world (e.g., 9/11 attack in U.S.A.—2982 caualities, Yazidi community bombings in Iraq—796 casualities, recent attack in Norway—77+ casualities, and bomb blasts, train explosions, plane bombings in Pakistan, India, U.K., Spain, and everywhere). www.wikipedia.org.
(20) Hrapovic, S.; Majid, E.; Liu, Y.; Male, K.; Luong, J. H. T. *Anal. Chem.* **2006**, *78*, 5504−5512.
(21) Wang, J.; Hocevar, S. B.; Ogorevc, B. *Electrochem. Commun.* **2004**, *6*, 176−179.
(22) Zhang, H.-X.; Cao, A.-M.; Hu, J.-S.; Wan, L.-J.; Lee, S.-T. *Anal. Chem.* **2006**, *78*, 1967−1971.
(23) Tang, L.; Feng, H.; Cheng, J.; Li, J. *Chem. Commun.* **2010**, *46*, 5882−5884.
(24) Walker, J. E.; Kaplan, D. L. *Biodegradation* **1992**, *3*, 369−385.
(25) Riskin, M.; Tel-Vered, R.; Bourenko, T.; Granot, E.; Willner, I. *J. Am. Chem. Soc.* **2008**, *130*, 9726−9733.
(26) Bozic, R. G.; West, A. C.; Levicky, R. *Sens. Actuators, B* **2008**, *133*, 509−515.
(27) Burrell, A. K.; Sesto, R. E. D.; Baker, S. N.; McCleskey, T. M.; Baker, G. A. *Green Chem.* **2007**, *9*, 449−454.
(28) Munch, J. C.; Petter, H. H. *J. Am. Pharm. Assoc.* **1965**, *5*, 493−494.
(29) Esteve-Nunez, A.; Caballero, A.; Ramos, J. L. *Microbiol. Mol. Biol. Rev.* **2001**, *65*, 335−352.
(30) Spain, J. C. *Annu. Rev. Microbiol.* **1995**, *49*, 523−555.
(31) Wang, J. *Electroanalysis* **2007**, *19*, 415−423.
(32) Zhang, H.-X.; Hu, J.-S.; Yan, C.-J.; Jiang, L.; Wan, L.-J. *Phys. Chem. Chem. Phys.* **2006**, *8*, 3567−3572.
(33) Bonhôte, P.; Dias, A.-P.; Papageorgiou, N.; Kalyanasundaram, K.; Grätzel, M. *Inorg. Chem.* **1996**, *35*, 1168−1178.
(34) Dieter, K. M.; Dymek, C. J.; Heimer, N. E.; Rovang, J. W.; Wilkes, J. S. *J. Am. Chem. Soc.* **1988**, *110*, 2722−2726.
(35) Scheiner, S.; Grabowski, S. J.; Kar, T. *J. Phys. Chem. A* **2001**, *105*, 10607−10612.
(36) Crowhurst, L.; Mawdsley, P. R.; Perez-Arlandis, J. M.; Salter, P. A.; Welton, T. *Phys. Chem. Chem. Phys.* **2003**, *5*, 2790−2794.
(37) Dutt, G. B. *J. Phys. Chem. B* **2010**, *114*, 8971−8977.
(38) Zhao, Q.; Eichhorn, J.; Pitner, W.; Anderson, J. *Anal. Bioanal. Chem.* **2009**, *395*, 225−234.
(39) Rooney, D.; Jacquemin, J.; Gardas, R.; Kirchner, B. *Top. Curr. Chem.* **2009**, *290*, 185−212.
(40) Ghatee, M. H.; Zare, M.; Moosavi, F.; Zolghadr, A. R. *J. Chem. Eng. Data* **2010**, *55*, 3084−3088.
(41) Marken, F.; Tsai, Y.-C.; Coles, B. A.; Matthews, S. L.; Compton, R. G. *New J. Chem.* **2000**, *24*, 653−658.
(42) Sun, J.-J.; Guo, L.; Zhang, D.-F.; Yin, W.-H.; Chen, G.-N. *Electrochem. Commun.* **2007**, *9*, 283−288.
(43) Forzani, E. S.; Lu, D.; Leright, M. J.; Aguilar, A. D.; Tsow, F.; Iglesias, R. A.; Zhang, Q.; Lu, J.; Li, J.; Tao, N. *J. Am. Chem. Soc.* **2009**, *131*, 1390−1391.